HUPD-9911
August 1999
Revised October 1999

Redshift-space Distortions of the Power Spectrum of Cosmological Objects on a Light Cone : Explicit Formulations and Theoretical Implications

Hiroaki NISHIOKA and Kazuhiro YAMAMOTO
Department of Physics, Hiroshima University, Higashi-Hiroshima 739-8526, Japan

ABSTRACT

We examine the effects of the linear and the cosmological redshift-space distortions on the power spectrum of cosmological objects on a light cone. We develop theoretical formulae for the power spectrum in linear theory of density perturbations in a rigorous manner starting from first principle corresponding to Fourier analysis. Approximate formulae, which are useful properly to incorporate the redshift-space distortion effects into the power spectrum are derived, and the validity is examined. Applying our formulae to galaxy and quasar samples which roughly match the SDSS survey, we will show how the redshift-space distortions distort the power spectrum on the light cone quantitatively.

Subject headings: cosmology: theory - dark matter - large-scale structure of universe – galaxies: distances and redshifts – quasars: general

1. INTRODUCTION

The wide-field redshift surveys of galaxies and quasars, like the Two-degree Field (2dF) and the Sloan Digital Sky Survey (SDSS), are key projects in the area of observational cosmology. These surveys provide three dimensional maps of the distribution of cosmological objects extended to high redshifts. The spatial distribution of the objects depends on various properties of the universe such as, initial density fluctuations, formation process of the cosmological objects, bias mechanism, luminosity function, cosmological parameters, and dark matter. The comparison of the observational data with theoretical predictions will put serious constraints on the cosmological

models. Especially the precise measurement of the power spectrum from the galaxy surveys is a promising project for the cosmological parameters and the initial density fluctuations, as well as the measurement of the cosmic microwave background anisotropies.

Two-point correlation function and the power spectrum are the most used tools to quantify the clustering of the cosmological objects. From a theoretical point of view, these statistical quantities that are well defined on the constant-time hypersurface have been used so far. However, cosmological observations are carried out only on a light cone. This fact requires statistical quantities which properly incorporate the light-cone effect. For the 2dF and SDSS surveys the light-cone effect becomes important because of the depth of the samples. This importance of the light-cone effect was discussed by several authors (Matarrese et al. 1997; Matsubara, Suto, & Szapudi 1997; Nakamura, Matsubara, & Suto 1998; de Laix & Starkman 1998; Moscardini et al. 1998). Recently, a rigorous framework to incorporate the light-cone effect into the two-point correlation function and the power spectrum has been developed (Yamamoto & Suto 1999, Papar I; Nishioka & Yamamoto 1999, Paper II; Suto et al. 1999 ; Yamamoto, Nishioka, & Suto 1999, Paper III).

The other important observational effect is the redshift-space distortion. Because cosmological surveys are carried out in redshift space, the peculiar velocity of sources distorts the distribution of the cosmological objects. This effect has been extensively investigated in linear theory (Davis & Peebles 1983; Kaiser 1987; Hamilton 1998; Szalay, Matsubara, & Landy 1998) and also in a nonlinear regime (Cole, Fisher, & Weinberg 1994; Suto, et al 1999; Magira, Jing, & Suto 1999). It has been also pointed out that the geometrical effect originating from the expansion of the universe causes another apparent distortion in the distribution of cosmological objects, i.e., cosmological redshift-space distortion (Alcock & Paczynski 1979; Ryden 1995; Matsubara & Suto 1996; Ballinger, Peacock, & Heavens 1996; Suto, et al 1999; Magira, Jing, & Suto 1999; Matsubara 1999). Though the authors in these previous works have focused on determining the cosmological parameters by using the cosmological redshift-space distortion, we note that the cosmological redshift-space distortion gives rise to a problem in determining the power spectrum because the cosmological parameters of the universe have not been well established.

In this paper we focus on the power spectrum on a light cone, taking into account the redshift-space distortion effects. We derive formulae for the power spectrum in a rigorous manner and examine how these effects distort the power spectrum measured in wide- and deep-field surveys. We adopt the following strategy. We first define an estimator for the power spectrum which can be computed from a sample of cosmological sources on a light cone, according to the conventional Fourier analysis. Then we calculate the ensemble average of the estimator, which we define the power spectrum on a light cone. Comparing this with the conventional power spectrum defined on a constant-time hypersurface in real space, we show how the distortion appears in the shape of the power spectrum on the light cone quantitatively, modeling galaxy and quasar samples which roughly match the SDSS samples.

In the present paper we work in linear theory, which enables us to derive formulae in a rigorous manner. However, this limits the validity of our results only to the large scales because the nonlinear effect affects the clustering features on the small scales. So the extension to include the nonlinear effect is needed, and a plausible extension is discussed in Paper Ⅲ.

This paper is organized as follows: In §2 we define the statistical estimators of the power spectrum and the two-point correlation function on a light cone. We will find that a familiar conventional relation between the power spectrum and the two-point correlation function, which is defined on a constant-time hypersurface, holds even for those thus defined on the light cone. In §3 we consider the linear redshift-space distortion effect on the power spectrum. Some parts in this section have been discussed in Paper Ⅲ. However, the approximate formula to incorporate the linear redshift-space distortion, which was introduced in Paper Ⅲ in an intuitive manner, is derived in the rigorous manner in the present section. And the validity of the approximate formula is examined in detail assuming galaxy and quasar samples. In §4 we consider the cosmological redshift-space distortion effect. Then the rigorous and the approximate formulae for the power spectrum on the light cone are derived. Then we examine the validity of approximation, and discuss the theoretical implications. §5 is devoted to summary and conclusions. Throughout this paper we use the unit in which the light velocity c equals 1.

For definiteness, we adopt notations similar to those in Paper Ⅲ, and use a superscript LC to indicate quantities on the light cone explicitly. The power spectrum without the superscript $P(k)$ denotes the CDM power spectrum defined on a constant-time hypersurface at present. And we use subscripts (superscripts) R and S to indicate quantities in real and redshift spaces, respectively.

2. DEFINITION OF THE POWER SPECTRUM

In this section we first define statistical estimators for the two-point correlation function and the power spectrum of cosmological objects on a light-cone hypersurface defined by an observer in redshift space. We define the statistical estimators for the two-point correlation function and the power spectrum, independently, which can be computed when a set of a survey catalog is obtained. Then we will show that a familiar fundamental relation holds between thus defined two-point correlation function and the power spectrum.

In a redshift survey, a position of a cosmological object is specified by the redshift z and the direction (unit) vector $\boldsymbol{\gamma}$. Cosmological distance to the object is evaluated from the redshift z through some converting formula. And a map of the cosmological objects is obtained. The statistical quantities, the power spectrum and the two-point correlation function, are computed from the map. By introducing the variable s to specify the cosmological distance (the radial coordinate) in redshift space, we write the number density field of the cosmological objects

in redshift space $n^{\rm S}(s,\boldsymbol{\gamma})$ and the mean number density $\tilde{n}^{\rm S}(s)$. [1] Following the conventional treatment of the power spectrum (e.g., Feldman, Kaiser, & Peacock 1994), we introduce the number density field

$$F(s,\boldsymbol{\gamma}) = \frac{n^{\rm S}(s,\boldsymbol{\gamma}) - n^{\rm S}_{\rm syn}(s,\boldsymbol{\gamma})}{\left[\int d^3\boldsymbol{s}\tilde{n}^{\rm S}(s)^2\right]^{\frac{1}{2}}}, \tag{1}$$

where $n^{\rm S}_{\rm syn}(s,\boldsymbol{\gamma})$ is the number density field of objects for a synthetic catalog without structure which has the same mean number density $\tilde{n}^{\rm S}(s)$ as that of the cosmological objects $n^{\rm S}(s,\boldsymbol{\gamma})$. To be specific for the synthetic catalog, if we write $n^{\rm S}(s,\boldsymbol{\gamma})$ and $n^{\rm S}_{\rm syn}(s,\boldsymbol{\gamma})$ as

$$n^{\rm S}(s,\boldsymbol{\gamma}) = \tilde{n}^{\rm S}(s)[1+\Delta^{\rm S}(s,\boldsymbol{\gamma})], \tag{2}$$

$$n^{\rm S}_{\rm syn}(s,\boldsymbol{\gamma}) = \tilde{n}^{\rm S}(s)[1+\Delta^{\rm S}_{\rm syn}(s,\boldsymbol{\gamma})], \tag{3}$$

respectively, we write

$$\Big\langle \Delta^{\rm S}_{\rm syn}(s_1,\boldsymbol{\gamma}_1)\Delta^{\rm S}_{\rm syn}(s_2,\boldsymbol{\gamma}_2)\Big\rangle = \Big\langle \Delta^{\rm S}(s_1,\boldsymbol{\gamma}_1)\Delta^{\rm S}_{\rm syn}(s_2,\boldsymbol{\gamma}_2)\Big\rangle = 0. \tag{4}$$

When the density field $F(s,\boldsymbol{\gamma})$ is given, one may compute the following two-point statistics,

$$\xi^{obs}(R) = \int \frac{d\Omega_{\hat{\boldsymbol{R}}}}{4\pi}\int d^3\boldsymbol{s}_1\int d^3\boldsymbol{s}_2 F(s_1,\boldsymbol{\gamma}_1)F(s_2,\boldsymbol{\gamma}_2)\delta^{(3)}(\boldsymbol{s}_1-\boldsymbol{s}_2-\boldsymbol{R}), \tag{5}$$

where $\boldsymbol{s}_1 = s_1\boldsymbol{\gamma}_1$ and $\boldsymbol{s}_2 = s_2\boldsymbol{\gamma}_2$ and $R = |\boldsymbol{R}|$, and $\hat{\boldsymbol{R}} = \boldsymbol{R}/R$. Note that this definition of the estimator for the two-point correlation function is slightly different from that in the previous paper (Paper I; Paper II). However, we will show that the difference is not practical and that the same formula is derived in the limit of the distant observer approximation (equation [29]).

Here $\xi^{obs}(R)$ is a mathematical expression for the two-point correlation function computed from a conventional data processing for a set of data $n^{\rm S}(s,\boldsymbol{\gamma})$ (for an observer). As is well-known as the problem of the cosmic variance, we can only predict the ensemble average of the statistical estimator, where the ensemble average means to average the estimator over many universes for different observers. Assuming that the selection function does not depend on the direction $\boldsymbol{\gamma}$, the ensemble average of the estimator is written as

$$\xi^{\rm LC}_{\rm S}(R) = \Big\langle \xi^{obs}(R)\Big\rangle = \int \frac{d\Omega_{\hat{\boldsymbol{R}}}}{4\pi}\int d^3\boldsymbol{s}_1\int d^3\boldsymbol{s}_2\Big\langle F(s_1,\boldsymbol{\gamma}_1)F(s_2,\boldsymbol{\gamma}_2)\delta^{(3)}(\boldsymbol{s}_1-\boldsymbol{s}_2-\boldsymbol{R})\Big\rangle, \tag{6}$$

which we define as the two-point correlation function on a light cone in redshift space.

Next we consider the power spectrum. When the density field $F(s,\boldsymbol{\gamma})$ is given, one can compute the Fourier coefficient of equation (1)

$$\mathcal{F}(\boldsymbol{k}) = \int d^3\boldsymbol{s}F(s,\boldsymbol{\gamma})e^{i\boldsymbol{k}\cdot\boldsymbol{s}} = \frac{\int d^3\boldsymbol{s}[n^{\rm S}(s,\boldsymbol{\gamma}) - n^{\rm S}_{\rm syn}(s,\boldsymbol{\gamma})]e^{i\boldsymbol{k}\cdot\boldsymbol{s}}}{\left[\int d^3\boldsymbol{s}\tilde{n}^{\rm S}(s)^2\right]^{\frac{1}{2}}}, \tag{7}$$

[1] We assume infinitely thin binwidth for the 'observed' data set.

and the power spectrum may be computed as follows (Feldman, Kaiser, & Peacock 1994),

$$P^{obs}(k) = \int \frac{d\Omega_{\hat{\boldsymbol{k}}}}{4\pi} |\mathcal{F}(\boldsymbol{k})|^2, \tag{8}$$

where $\boldsymbol{k}$ denotes the wavenumber vector, $k = |\boldsymbol{k}|$, and $\hat{\boldsymbol{k}} = \boldsymbol{k}/k$. Similar to the case of the two-point correlation function, $P^{obs}(k)$ models a conventional estimation of the power spectrum computed from a set of data $F(s, \boldsymbol{\gamma})$ for an observer. The ensemble average of the statistical estimator is written as

$$P_{\rm S}^{\rm LC}(k) = \Big\langle P^{obs}(k) \Big\rangle = \int \frac{d\Omega_{\hat{\boldsymbol{k}}}}{4\pi} \Big\langle |\mathcal{F}(\boldsymbol{k})|^2 \Big\rangle, \tag{9}$$

which we define as the power spectrum on a light cone in redshift space (see also Paper III).

When we adopt the above definitions, we show the familiar fundamental relation which holds between the two-point correlation function and the power spectrum, as follows. With the use of the relation

$$\delta^{(3)}(\boldsymbol{s}_1 - \boldsymbol{s}_2 - \boldsymbol{R}) = \int \frac{d^3\boldsymbol{k}}{(2\pi)^3} e^{i\boldsymbol{k}\cdot(\boldsymbol{s}_1 - \boldsymbol{s}_2 - \boldsymbol{R})}, \tag{10}$$

equation (6) is written as

$$\begin{aligned} \xi_{\rm S}^{\rm LC}(R) &= \int \frac{d\Omega_{\hat{\boldsymbol{R}}}}{4\pi} \int \frac{d^3\boldsymbol{k}}{(2\pi)^3} \Big\langle |F(\boldsymbol{k})|^2 \Big\rangle e^{-i\boldsymbol{k}\cdot\boldsymbol{R}} \\ &= \frac{1}{2\pi^2} \int dk k^2 P_{\rm S}^{\rm LC}(k) j_0(kR). \end{aligned} \tag{11}$$

The inverse Fourier transformation yields,

$$P_{\rm S}^{\rm LC}(k) = 4\pi \int dR R^2 \xi_{\rm S}^{\rm LC}(R) j_0(kR). \tag{12}$$

Equations (11) and (12) are the familiar formulae which hold for the conventional two-point correlation function and the power spectrum defined on a constant-time hypersurface.

3. LINEAR REDSHIFT-SPACE DISTORTION

The distortion due to the linear peculiar velocity field of cosmological objects is called as the linear redshift-space distortion. In this section we consider the linear redshift-space distortion under the assumption that the cosmological model is exactly determined. An error of assuming the cosmological model causes another distortion, i.e., the cosmological redshift-space distortion, which will be investigated in the next section.

3.1. Two-point correlation function on a light cone

In this subsection we first calculate the two-point correlation function, taking into account the linear redshift-space distortion. Formulation is developed within linear theory of density

perturbations based on the CDM scenario. Because the definition of the two-point correlation function is different from that in the previous paper (Papers II), derivation of the formula is slightly different from the previous one. We briefly summarize the calculation for definiteness.

Throughout the present paper, we consider the spatially-flat Friedmann-Lemaitre universe, whose line element is expressed as

$$ds^2 = a^2(\eta)\Big[-d\eta^2 + d\chi^2 + \chi^2 d\Omega^2_{(2)}\Big], \tag{13}$$

where η is the conformal time, a is the scale factor, χ is the radial coordinate, and $d\Omega^2_{(2)}$ is the line element of the unit two-sphere. We normalize the scale factor to be unity at present, $a(\eta_0) = 1$. Then the Friedmann equation is

$$\left(\frac{\dot{a}}{a}\right)^2 = H_0^2\left(\frac{\Omega_0}{a} + a^2\Omega_\lambda\right), \tag{14}$$

where $H_0 = 100h$km/s/Mpc is the Hubble parameter, $\Omega_0(= 1 - \Omega_\lambda)$ is the density parameter, and the dot denotes η-differentiation.

Since we locate a fiducial observer at the origin of coordinates ($\eta = \eta_0, \chi = 0$), a cosmological object at χ and η on the light cone hypersurface of the observer satisfies the simple relation $\eta = \eta_0 - \chi$. We introduce the radial coordinate r to express the three dimensional (real) space on the light-cone hypersurface, in which the position of a source is specified by $(r, \boldsymbol{\gamma})$, where $\boldsymbol{\gamma}$ is an unit vector along the line of sight. Essentially, r is equivalent to χ, however, we use r for mathematical conveniences and to represent that quantities are defined on the light cone explicitly. Then we denote the metric of the three dimensional space on the light cone as,

$$ds^2_{\rm LC} = dr^2 + r^2 d\Omega^2_{(2)}, \tag{15}$$

and we write the number density of sources on the light cone as $n^{\rm R}(r, \boldsymbol{\gamma})$, which is simply related to the comoving number density of objects at a conformal time η and at a position, $(\chi, \boldsymbol{\gamma})$, $n(\eta, \chi, \boldsymbol{\gamma})$ as

$$n^{\rm R}(r, \boldsymbol{\gamma}) = n(\eta, \chi, \boldsymbol{\gamma})|_{\eta\to\eta_0-r, \chi\to r}. \tag{16}$$

By using the mean observed comoving number density $\tilde{n}(\eta)$ at time η and the density fluctuation of luminous objects $\Delta(\eta, \chi, \boldsymbol{\gamma})$, we write

$$n(\eta, \chi, \boldsymbol{\gamma}) = \tilde{n}(\eta)[1 + \Delta(\eta, \chi, \boldsymbol{\gamma})]. \tag{17}$$

Then equation (16) is rewritten as

$$n^{\rm R}(r, \boldsymbol{\gamma}) = \tilde{n}^{\rm R}(r)[1 + \Delta^{\rm R}(r, \boldsymbol{\gamma})], \tag{18}$$

where we defined

$$\tilde{n}^{\rm R}(r) \equiv \tilde{n}(\eta)|_{\eta\to\eta_0-r}, \qquad \Delta^{\rm R}(r, \boldsymbol{\gamma}) \equiv \Delta(\eta, \chi, \boldsymbol{\gamma})|_{\eta\to\eta_0-r, \chi\to r}. \tag{19}$$

Note that the mean observed number density $\tilde{n}(\eta)$ is different from the mean number density of the objects at η by a factor of a selection function.

Now we consider the two-point correlation function (6) in redshift space. The relation between the redshift space and the real space is specified as follows,

$$n^{\rm S}(s,\boldsymbol{\gamma})s^2dsd\Omega_{\boldsymbol{\gamma}} = n^{\rm R}(r,\boldsymbol{\gamma})r^2drd\Omega_{\boldsymbol{\gamma}}, \tag{20}$$

$$n^{\rm S}_{\rm syn}(s,\boldsymbol{\gamma})s^2dsd\Omega_{\boldsymbol{\gamma}} = n^{\rm R}_{\rm syn}(r,\boldsymbol{\gamma})r^2drd\Omega_{\boldsymbol{\gamma}}, \tag{21}$$

and

$$s = r + \delta r(r,\boldsymbol{\gamma}), \tag{22}$$

where $\delta r(r,\boldsymbol{\gamma})$ in equation (22) represents the apparent shift in the comoving radial coordinate due to peculiar velocity. $\delta r(r,\boldsymbol{\gamma})$ is of order of the velocity perturbations, and the explicit expression is summarized in Appendix. Equation (21) defines the number density of the synthetic catalog in real space $n^{\rm R}_{\rm syn}(r,\boldsymbol{\gamma})$.

With the use of the above equations we obtain the following expression from equation (6),

$$\begin{aligned}\xi^{\rm LC}_{\rm S}(R) &= \left[\int d^3\boldsymbol{r}\tilde{n}^{\rm R}(r)^2\right]^{-1}\int\frac{d\Omega_{\hat{\mathbf{R}}}}{4\pi}\int dr_1r_1^2d\Omega_{\boldsymbol{\gamma}_1}\int dr_2r_2^2d\Omega_{\boldsymbol{\gamma}_2}\\ &\times\Big\langle[n^{\rm R}(r_1,\boldsymbol{\gamma}_1)-n^{\rm R}_{\rm syn}(r_1,\boldsymbol{\gamma}_1)][n^{\rm R}(r_2,\boldsymbol{\gamma}_2)-n^{\rm R}_{\rm syn}(r_2,\boldsymbol{\gamma}_2)]\\ &\times\delta^{(3)}(\boldsymbol{r}_1+\delta\boldsymbol{r}_1-\boldsymbol{r}_2-\delta\boldsymbol{r}_2-\boldsymbol{R})\Big\rangle,\end{aligned} \tag{23}$$

where $\boldsymbol{r}+\delta\boldsymbol{r} = (r+\delta r)\boldsymbol{\gamma}$, and we have assumed

$$\int d^3\boldsymbol{s}\tilde{n}^{\rm S}(s)^2 = \int d^3\boldsymbol{r}\tilde{n}^{\rm R}(r)^2. \tag{24}$$

Note that the number density field of the synthetic catalog in redshift space $n^{\rm S}_{\rm syn}(s,\boldsymbol{\gamma})$ has no structure. Then the number density field in real space $n^{\rm R}_{\rm syn}(r,\boldsymbol{\gamma})$, which is defined by equation (21), has a structure. Writing the number density field as

$$n^{\rm R}_{\rm syn}(r,\boldsymbol{\gamma}) = \tilde{n}^{\rm R}(r)[1+\Delta^{\rm R}_{\rm syn}(r,\boldsymbol{\gamma})], \tag{25}$$

the density contrast $\Delta^{\rm R}_{\rm syn}(r,\boldsymbol{\gamma})$ is expressed as (Hamilton 1998),

$$\Delta^{\rm R}_{\rm syn}(r,\boldsymbol{\gamma}) = \Delta^{\rm S}_{\rm syn}(r,\boldsymbol{\gamma}) + \left(\frac{\partial}{\partial r}+\frac{\kappa(r)}{r}\right)\delta r(r,\boldsymbol{\gamma}), \tag{26}$$

where

$$\kappa(r) = \frac{\partial\ln r^2\tilde{n}^{\rm R}(r)}{\partial\ln r}, \tag{27}$$

and we used $\Delta^{\rm S}_{\rm syn}(r,\boldsymbol{\gamma}) = \Delta^{\rm S}_{\rm syn}(s,\boldsymbol{\gamma})$, which holds within the linear order of perturbations. In the leading order of the perturbative expansion, equation (23) is rewritten as

$$\xi^{\rm LC}_{\rm S}(R) = \left[\int d^3\boldsymbol{r}\tilde{n}^{\rm R}(r)^2\right]^{-1}\int\frac{d\Omega_{\hat{\boldsymbol{R}}}}{4\pi}\int dr_1r_1^2d\Omega_{\boldsymbol{\gamma}_1}\int dr_2r_2^2d\Omega_{\boldsymbol{\gamma}_2}\tilde{n}^{\rm R}(r_1)\tilde{n}^{\rm R}(r_2)$$

$$\times\Big\langle[\Delta^{\rm R}(r_1,\boldsymbol{\gamma}_1)-\left(\frac{\partial}{\partial r_1}+\frac{\kappa(r_1)}{r_1}\right)\delta r_1(r_1,\boldsymbol{\gamma}_1)]$$
$$\times[\Delta^{\rm R}(r_2,\boldsymbol{\gamma}_2)-\left(\frac{\partial}{\partial r_2}+\frac{\kappa(r_2)}{r_2}\right)\delta r_2(r_2,\boldsymbol{\gamma}_2)]\Big\rangle\delta^{(3)}(\boldsymbol{r}_1-\boldsymbol{r}_2-\boldsymbol{R})\ , \tag{28}$$

where we used equations (18), (25), (26), and (4).

After straightforward calculations based on the CDM model with the linear biasing (equation [A8]), we obtain the following expression (see Appendix),

$$\begin{aligned}\xi_{\rm S}^{\rm LC}(R) &= \left[\int drr^2\tilde{n}^{\rm R}(r)^2\right]^{-1}\frac{1}{2R}\iint_{\mathcal{S}}dr_1dr_2r_1r_2\tilde{n}^{\rm R}(r_1)\tilde{n}^{\rm R}(r_2)\\
&\times\frac{1}{2\pi^2}\int dkk^2P(k)\prod_{i=1}^{2}\Big[b(k;\eta_0-r_i)D_1(\eta_0-r_i)\Big]\\
&\times\Big[j_0(kR)+\beta(k;\eta_0-r_2)I(k;R;r_1,r_2)+\beta(k;\eta_0-r_1)I(k;R;r_2,r_1)\\
&+\beta(k;\eta_0-r_1)\beta(k;\eta_0-r_2)J(k;R;r_1,r_2)\Big],\end{aligned} \tag{29}$$

where $\mathcal{S}$ denotes the region $|r_1-r_2|\le R\le r_1+r_2$, $P(k)$ is the CDM power spectrum at present, $D_1(\eta)$ is the linear growth rate normalized to be unity at present, $I(k;R;r_1,r_2)$ and $J(k;R;r_1,r_2)$ are defined by equations (A24) and (A25), respectively, and $\beta(k;\eta)$ is defined as

$$\beta(k;\eta)=\frac{1}{b(k;\eta)}\frac{d\ln D_1(\eta)}{d\ln a(\eta)}. \tag{30}$$

3.2. Distant Observer Approximation

As is shown in Paper II, equation (29) reduces to a simple form by applying the plane-parallel, or distant observer, approximation. In the case $R\ll 2r_{\rm max}$, where $2r_{\rm max}$ is the size of the survey volume, we can use the approximation

$$\iint_{\mathcal{S}}dr_1dr_2\simeq\int dr_1\int_{-R}^{R}dx \tag{31}$$

where $x=r_2-r_1$, and $I(k;R;r_1,r_2)$ and $J(k;R;r_1,r_2)$ are approximated as

$$I(k;R;r_1,r_2) = \frac{j_1(kR)}{kR}-\frac{j_2(kR)}{R^2}x^2, \tag{32}$$

$$J(k;R;r_1,r_2) = 3\frac{j_2(kR)}{(kR)^2}-6\frac{j_3(kR)}{kR^3}x^2+\frac{j_4(kR)}{R^4}x^4, \tag{33}$$

respectively. Integration over x yields,

$$\xi_{\rm S}^{\rm LC}(R)\simeq\frac{\int drr^2\tilde{n}^{\rm R}(r)^2\xi[R,z(r)]_{\rm source}}{\int drr^2\tilde{n}^{\rm R}(r)^2}, \tag{34}$$

where we defined

$$\xi[R,z(r)]_{\rm source} = \frac{1}{2\pi^2}\int dk k^2 P(k) D_1(\eta_0-r)^2 b(k;\eta_0-r)^2 \times\left[1+\frac{2}{3}\beta(k;\eta_0-r)+\frac{1}{5}\beta(k;\eta_0-r)^2\right] j_0(kR). \quad (35)$$

This formula indicates that the two-point correlation function on a light cone is obtained by averaging the correlation function at each time defined on a constant-time hypersurface $\xi[R,z(r)]_{\rm source}$ by weighting $\tilde{n}^{\rm R}(r)^2$. Note that this formula has been rigorously derived only in the framework of linear theory of density perturbations.

3.3. Power spectrum on a light cone

The power spectrum is obtained from the two-point correlation function as described in section 2. By substituting equation (29) into (12) we compute the power spectrum on the light cone $P_{\rm S}^{\rm LC}(k)$. Some aspects of the power spectrum on the light cone have been discussed in Paper Ⅲ. Although a different method was adopted to compute the power spectrum in Paper Ⅲ, we find that the approach employed in this paper is rather useful. We derive the simple expression for the power spectrum, which was used without detailed verification in Paper Ⅲ, and discuss the validity of approximation in subsection 3.5.

The approximate formula for the power spectrum is easily obtained by substituting equation (34) into (12),

$$P_{\rm S}^{\rm LC}(k) \simeq \alpha(k) P(k), \quad (36)$$

where

$$\alpha(k) = \frac{\displaystyle\int dr r^2 \tilde{n}^{\rm R}(r)^2 b(k;\eta_0-r)^2 D_1(\eta_0-r)^2\left[1+\frac{2}{3}\beta(k;\eta_0-r)+\frac{1}{5}\beta(k;\eta_0-r)^2\right]}{\displaystyle\int dr r^2 \tilde{n}^{\rm R}(r)^2}. \quad (37)$$

This equation justifies the extended formula (20) in Paper Ⅲ.

In the case that the bias does not depend on scales of density fluctuation or k, i.e., $b(k;\eta) = b(\eta)$, $\alpha(k)$ becomes a constant α. Thus in this case the light-cone effect and the linear redshift-space distortion are described by the constant α. In the small scales of large wavenumber of k, the nonlinearity distorts the power spectrum in redshift space, and produces an additional scale-dependence in the power spectrum on the light-cone. Importance of the nonlinearity in small scales is extensively discussed in Paper Ⅲ (see also Magira, Jing, & Suto 1999).

3.4. Model of samples

In subsection 3.5 we apply the formulae developed in the previous subsections to galaxy and quasar samples, and discuss the validity of approximation by comparing the approximate formula with the exact formula using numerical calculations. [2] For that purpose, we need to model galaxy and quasar samples and bias. For a galaxy luminosity function, we adopt a B-band luminosity function of the APM galaxies (Loveday et al. 1992) fitted to Schechter function

$$\phi(L)dL = \phi^*\Big(\frac{L}{L^*}\Big)^\nu \exp\Big(-\frac{L}{L^*}\Big)d\Big(\frac{L}{L^*}\Big), \tag{38}$$

with $\phi^* = 1.40 \times 10^{-2}h^3\mathrm{Mpc}^{-3}$, $\nu = -0.97$, and $M_B^* = -19.50 + 5\log_{10}h$. Then the comoving number density of galaxies at z which are brighter than the limiting magnitude $B_{\rm lim}$ is given by

$$\tilde{n}(z, < B_{\rm lim}) = \int_{L(B_{\rm lim},z)}^{\infty} \phi(L)dL = \phi^*\Gamma[\nu+1, x(B_{\rm lim}, z)], \tag{39}$$

where

$$x(B_{\rm lim}, z) = \frac{L(B_{\rm lim}, z)}{L^*} = \Big[\frac{d_L(z)}{1h^{-1}\mathrm{Mpc}}\Big]^2 10^{2.2-0.4B_{\rm lim}}, \tag{40}$$

and $\Gamma[\nu, x]$ is the incomplete Gamma function. We consider the galaxy sample in the range of redshift $0 \le z \le 0.2$, and adopt the B-band limiting magnitude 19 to match the SDSS spectroscopic sample.

We also assume quasar samples which roughly match the SDSS quasar survey, where we use a selection function for B-band magnitude limited samples on the basis of the luminosity function by Wallington & Narayan (1993) and adopt the B-band limiting magnitude 20 (see also Nakamura & Suto 1997; Paper I). And we assume the depth of the survey volume, $z_{\rm max} = 5$.

As for the bias, we adopt the simple scale-independent model (Paper Ⅲ), which is a phenomenological extension of the Fry's bias model (1996),

$$b(\eta) = 1 + \frac{1}{[D_1(\eta)]^p}(b_0 - 1), \tag{41}$$

where $b_0 = b(\eta_0)$ is the bias parameter at present, and p is the constant which controls time-evolution. Note that this model reduces to the case of no bias when the constant b_0 is unity and that the case $p = 1$ is equivalent to the model by Fry (1996).

We consider the SCDM(standard cold dark matter) and the LCDM(Lambda cold dark matter) models, which have $(\Omega_0, \Omega_\lambda, h, \sigma_8) = (1.0, 0.0, 0.5, 0.56)$ and $(0.3, 0.7, 0.7, 1.0)$, respectively. We

[2]The terminology, 'exact' formula, means the exact expression rigorously derived from definition (6) or (9) within the linear theory of density perturbation and bias. And the 'approximate' formula means its version in the distant observer limit. In a realistic situation, the nonlinearity of density perturbations and complex features of bias cause additional deformation of the power spectrum. (See also Paper Ⅲ, in which some aspects of the nonlinear effects are discussed.)

assume the Harrison-Zel'dovich initial power spectrum. The sets of the cosmological parameters are chosen so as to reproduce the observed cluster abundance (Kitayama & Suto 1997). And we use the CDM transfer function (Bardeen et al.1986; Sugiyama 1995) with $\Omega_b h^2 = 0.015$ in this section. Then the CDM power spectrum at present time is written as

$$P(k) = BkT(k)^2, \tag{42}$$

where

$$T(k) = \frac{\ln[1+2.34q]}{2.34q[1+3.89q+(16.1q)^2+(5.46q)^3+(6.71q)^4]^{1/4}} \tag{43}$$

and

$$q = \left(\frac{2.726}{2.7}\right)^2 \frac{k}{\Omega_0 h \exp[-\Omega_b - \sqrt{2h}\Omega_b/\Omega_0] h\mathrm{Mpc}^{-1}}, \tag{44}$$

where B is a normalization constant.

3.5. Validity of approximation and implications

To compute the exact power spectrum on a light-cone, we first perform integration of equation (29), and obtain the two-point correlation function $\xi_{\rm S}^{\rm LC}(R)$. Then we compute the power spectrum by using equation (12). As an example to show typical behavior of the two-point correlation function, Figure 1 plots the galaxy two-point correlation function in the LCDM model. Here we adopt the case of no bias, i.e., $b_0 = 1$ in (41). The solid line, which represents the exact two-point correlation function (29), is compared with the dotted line, which represents the approximate formula (34). The exact two-point correlation function shows a good correspondence with the approximate formula at small R. However the deviation becomes significant at large R and the exact two-point correlation function drops down to zero at the point, where R becomes two times of the depth of the survey volume (diameter of the survey volume), i.e., $2r_{\rm max}(z_{\rm max})$. This is traced back to our definition of the two-point correlation function. Namely number density outside the survey region is zero, then a product of the number density of the two points being $R > 2r_{\rm max}(z_{\rm max})$ must be zero.

Now we discuss the power spectrum. Figure 2 plots the galaxy power spectra to show characteristic behaviors, in which we adopted the LCDM model and the case of no bias. The solid line, which represents the exact power spectrum, is compared with the dotted line, which represents the approximate formula (36). Comparing the exact and the approximate power spectra, we see that the approximation is fairly good for $k \gtrsim 0.01h\mathrm{Mpc}^{-1}$. On the larger scales, the exact power spectrum approaches a constant value, and the deviation between the exact and the approximate formulae becomes large. This behavior originates from the fact that the corresponding wavelength becomes larger than depth of the survey volume at the large scales, $1/k \gtrsim r_{\rm max}$, and that we cannot properly evaluate the power spectrum because of the finite size effect of the survey volume. For comparison, the CDM power spectrum defined on a constant-time

hypersurface at present is plotted (dashed line). Note that in this case the CDM power spectrum is identical to the galaxy power spectrum on the constant-time hypersurface because we have adopted the case of no bias.

To quantify validity of the approximate formula, Figure 3 plots the power spectra for the galaxy and quasar samples, which are divided by the power spectrum on the constant-time hypersurface at present. The solid line expresses the exact power spectrum and the dotted line does the approximate one (36) in redshift space. For comparison we show the case in real space, where we refer the 'real space' to the case $\beta(k;\eta) = 0$ in the formulae. The short and the long dashed lines express the exact and the approximate power spectra, respectively, in real space. It is apparent from Figure 3 that the galaxy power spectrum is increased by the linear redshift-space distortion which dominantly contributes to the galaxy sample. The light-cone effect is not so effective for the galaxy sample because the sample is shallow. Nevertheless it can be notable that the light-cone effect decreases the amplitude of the power spectrum by order of several percent. On the other hand, the quasar power spectrum is significantly decreased because the light-cone effect is effective for such a deep observational field. However we should remind that the behavior of the power spectrum significantly depends on the time-dependence of the bias, which determines the amplitude of clustering at high-redshift (see also Figure 4). In each panel, we see that the approximation reproduces the exact power spectra fairly well for $k \gtrsim 0.01h\mathrm{Mpc}^{-1}$ for the galaxies and quasars samples. Thus we conclude that equation (36) provide a good approximate formula for the power spectrum on the light cone for $k \gtrsim 0.01h\mathrm{Mpc}^{-1}$.

Here we briefly mention the nonlinear effects on the power spectrum. While the nonlinear evolution of density field enhances the amplitude, the finger-of-God due to the random motion decreases the amplitude in redshift space. According to the result in Paper Ⅲ, the amplitude is decreased by order of several $\times 10\%$ relative to its counterpart in linear theory for both galaxy and quasar samples, depending on the scale k and the cosmological model. This situation is clearly shown in Figure 2 in Paper Ⅲ, from which we see that the nonlinear effects are effective for $k \gtrsim 0.1h\mathrm{Mpc}^{-1}$. Because we have not taken the nonlinear effects into account throughout the present paper, Figure 3 in the present paper does not show the decrease of the amplitude at the small scales. The difference between the Figure 3 and Figure 2 in Paper Ⅲ at small k is caused by the finite size effect of survey volume.

Finally in this section we discuss dependence of cosmology. Figure 4 plots the factor α/b_0^2 as a function of Ω_0, where α is defined by equation (37). The solid and the dotted lines represent the factor α/b_0^2 in redshift space and real space, respectively. Here we adopt the same model for the galaxy and quasar samples as in Figure 3. From Figure 4 it is apparent that the light-cone effect and the linear redshift-space distortion becomes more influential as Ω_0 increases. This will be traced back to the linear growth rate of density perturbations. For the galaxy sample, the increase of amplitude due to the redshift-space distortion is more effective than the decrease due to the light-cone effect. In contrast to this, for the quasar sample, the light-cone effect and the time-evolution of the bias become important.

4. COSMOLOGICAL REDSHIFT-SPACE DISTORTION

The crucial point of our investigation in the previous section is the assumption that we know the exactly correct cosmological model of the universe. Because the redshift z and the direction $\boldsymbol{\gamma}$ are the observable quantities of objects in the redshift survey, then we must assume a cosmological model to obtain a three-dimensional map on which the cosmological objects are plotted. Since the cosmological parameters of our universe have not been established completely, then we should be careful for this uncertainty.

It is known that an apparent shape of distribution of cosmological objects is distorted by the cosmological redshift-space distortion. The cosmological redshift-space distortion has been discussed as a tool for the cosmological model (Alcock & Paczynski 1979; Ryden 1995; Ballinger, Peacock, & Heavens 1996; Matsubara & Suto 1996; Suto, et al. 1999; Magira, Jing, & Suto 1999). An incorrect assumption of the cosmological model affects proper estimation of the two-point correlation function and the power spectrum. In this section we focus on this point and we investigate how the error of the assumption of cosmological model affects the estimation of the power spectrum on a light cone.

4.1. Basic Formulation

In this section, we assume that the universe is the Friedmann-Lemaitre universe with a cosmological constant and that the 'correct' matter density parameter is Ω_0. We also assume that data processing is performed by assuming the Friedmann-Lemaitre universe with an 'incorrect' matter density parameter $\bar{\Omega}_0$. In this section we neglect the effect of the linear redshift-space distortion for simplicity. In this case, the real space is the universe with the 'correct' density parameter Ω_0, and is described by the same relations in the previous section. And we use the same notations from equation (13) to (19) to describe the real space. On the other hand, the redshift space is the universe with the 'incorrect' density parameter $\bar{\Omega}_0$. To describe the redshift space, we write the line element

$$ds^2 = \bar{a}^2(\bar{\eta})\left[-d\bar{\eta}^2 + d\bar{\chi}^2 + \bar{\chi}^2 d\Omega^2_{(2)}\right], \tag{45}$$

where $\bar{a}(\bar{\eta})$ is the scale factor normalized to be unity at present, i.e., $\bar{a}(\bar{\eta}_0) = 1$, $\bar{\eta}$ is the conformal time, $\bar{\chi}$ is the radial coordinate, and and $d\Omega^2_{(2)}$ denotes the line element of the unit two-sphere. Evolution of the scale factor $\bar{a}$ is specified by the similar equation as (14),

$$\left(\frac{1}{\bar{a}}\frac{d\bar{a}}{d\bar{\eta}}\right)^2 = \bar{H}_0^2\left(\frac{\bar{\Omega}_0}{\bar{a}} + \bar{a}^2\bar{\Omega}_\lambda\right), \tag{46}$$

where $\bar{\Omega}_\lambda = 1 - \bar{\Omega}_0$, and $\bar{H}_0 = 100\bar{h}$km/s/Mpc is the Hubble parameter in redshift space. As in subsection 3.1, we assume that an observer is located at the origin of the coordinates ($\bar{\eta} = \bar{\eta}_0, \bar{\chi} = 0$), and the light-cone hypersurface of the observer satisfies the relation $\bar{\eta} = \bar{\eta}_0 - \bar{\chi}$. Then we introduce the radial coordinate s to denote the metric of the three dimensional

redshift-space on the light-cone hypersurface as

$$d\bar{s}^2_{\rm LC} = ds^2 + s^2 d\Omega^2_{(2)}. \tag{47}$$

The relation between z and s is specified by $\bar{a}(\bar{\eta}_0 - s) = 1/(1+z)$. When a set of data $(z, \boldsymbol{\gamma})$ for cosmological objects was obtained, we compute the number density field $F(s, \boldsymbol{\gamma})$ defined by equation (1) with the number density field $n^{\rm S}(s, \boldsymbol{\gamma})$ and that for a synthetic catalog $n^{\rm S}_{\rm syn}(s, \boldsymbol{\gamma})$. And a map is constructed in redshift space (47). Then we can compute the two-point correlation function and the power spectrum, according as the definitions (6) and (9), respectively. We specify relations between the redshift space and the real space, as is done in subsection 3.1. The relation for the number density field is specified by the same equations as (20) and (21). The relation between s and r is specified by

$$a(\eta_0 - r) = \bar{a}(\bar{\eta}_0 - s) = \frac{1}{1+z}, \tag{48}$$

where $a(\eta)$ and $\bar{a}(\bar{\eta})$ are the solutions of equations (14) and (46), respectively.

Now we calculate the two-point correlation function. With the use of equations, (20), (21), and (18), we find that (6) reduces to

$$\xi^{\rm LC}_{\rm S}(R) = \frac{\displaystyle\int \frac{d\Omega_{\hat{\boldsymbol{R}}}}{4\pi} \int d^3\boldsymbol{r}_1 \int d^3\boldsymbol{r}_2 \tilde{n}^{\rm R}(r_1)\tilde{n}^{\rm R}(r_2) \Big\langle \Delta^{\rm R}(r_1, \boldsymbol{\gamma}_1)\Delta^{\rm R}(r_2, \boldsymbol{\gamma}_2)\Big\rangle \delta^{(3)}(\boldsymbol{s}_1 - \boldsymbol{s}_2 - \boldsymbol{R})}{\displaystyle\int d^3\boldsymbol{r} \left(\frac{dr}{ds}\right)\left(\frac{r}{s}\right)^2 \tilde{n}^{\rm R}(r)^2}, \tag{49}$$

where we used $\tilde{n}^{\rm S}(s)s^2 ds = \tilde{n}^{\rm R}(r)r^2 dr$ to write the denominator.

After straightforward calculations similar to those in Appendix, we find that the above expression reduces to

$$\begin{aligned}\xi^{\rm LC}_{\rm S}(R) = &\left[4\pi \int dr r^2 \left(\frac{dr}{ds}\right)\left(\frac{r}{s}\right)^2 \tilde{n}^{\rm R}(r)^2\right]^{-1} \\ &\times \frac{1}{\pi R} \int\int_{\mathcal{M}} dr_1 dr_2 \prod_{j=1}^{2} \left(\frac{r_j^2}{s_j}\tilde{n}^{\rm R}(\eta_0 - r_j) D_1(\eta_0 - r_j)\right) \\ &\times \int dk k^2 P(k) b(k; \eta_0 - r_1) b(k; \eta_0 - r_2) j_0\left(k\sqrt{r_1^2 + r_2^2 - r_1 r_2 \frac{s_1^2 + s_2^2 - R^2}{s_1 s_2}}\right),\end{aligned} \tag{50}$$

where $\mathcal{M}$ denotes the region $|s_1 - s_2| \le R \le s_1 + s_2$, and s_1 and s_2 are understood as functions of r_1 and r_2, respectively, which are specified by equation (48). Thus the formula (50) is the exact two-point correlation function which takes the cosmological redshift-space distortion into account. Note that (50) reduces to the two-point correlation function in real space $\xi^{\rm LC}_{\rm R}(R)$, which is explicitly defined by (29) with setting $\beta(k;\eta) = 0$, when the 'correct' cosmological model is chosen as the redshift space, i.e., $\Omega_0 = \bar{\Omega}_0$ and $h = \bar{h}$.

4.2. Distant observer approximation

We consider an approximate expression of (50) in the simlar way to subsection 3.2. We introduce the variables $y = s_2 - s_1$ and $x = r_2 - r_1$, and set that $y \ll s_1, s_2$ and $x \ll r_1, r_2$. In this case the argument of the spherical bessel function in (50) is approximated as

$$k\sqrt{r_1^2 + r_2^2 - r_1 r_2 \frac{s_1^2 + s_2^2 - R^2}{s_1 s_2}} \simeq k\sqrt{\frac{r_1^2}{s_1^2}R^2 + \left[\left(\frac{dr_1}{ds_1}\right)^2 - \frac{r_1^2}{s_1^2}\right]y^2}, \tag{51}$$

where we used

$$\frac{x}{y} = \frac{r_2 - r_1}{s_2 - s_1} \simeq \frac{dr_1}{ds_1}. \tag{52}$$

Taking s_1 and y as the integration variables instead of r_1 and r_2 in (50), and we use the approximation,

$$\int\int_{\mathcal{M}} ds_1 ds_2 \simeq \int ds_1 \int_{-R}^{R} dy. \tag{53}$$

Introducing the new variable μ instead of y by $\mu = y/R$, then (50) is approximated as

$$\begin{aligned}\xi_{\rm S}^{\rm LC}(R) \simeq & \left[4\pi \int ds s^2 \left(\frac{dr}{ds}\right)^2 \left(\frac{r}{s}\right)^4 \tilde{n}^{\rm R}(r)^2\right]^{-1} \\ & \times \frac{1}{\pi}\int ds_1 \int_{-1}^{1} d\mu \left(\frac{dr_1}{ds_1}\right)^2 \left(\frac{r_1^2}{s_1}\right)^2 \Big[\tilde{n}^{\rm R}(\eta_0 - r_1) D_1(\eta_0 - r_1)\Big]^2 \\ & \times \int dk k^2 P(k) b(k; \eta_0 - r_1)^2 j_0\Big(kR\Theta\Big),\end{aligned} \tag{54}$$

where we defined

$$\Theta = \sqrt{\frac{r_1^2}{s_1^2} + \left[\left(\frac{dr_1}{ds_1}\right)^2 - \frac{r_1^2}{s_1^2}\right]\mu^2}. \tag{55}$$

Substituting equation (54) into (12), one obtains

$$\begin{aligned}P_{\rm S}^{\rm LC}(k) \simeq & \left[\int ds s^2 \left(\frac{dr}{ds}\right)^2 \left(\frac{r^2}{s^2}\right)^2 \tilde{n}^{\rm R}(r)^2\right]^{-1} \\ & \times \int ds_1 s_1^2 \left(\frac{dr_1}{ds_1}\right)^2 \left(\frac{r_1^2}{s_1^2}\right)^2 \Big[\tilde{n}^{\rm R}(\eta_0 - r_1) D_1(\eta_0 - r_1)\Big]^2 \\ & \times \int_0^1 d\mu P\Big(\frac{k}{\Theta}\Big) \frac{b\Big(k/\Theta; \eta_0 - r_1\Big)^2}{\Theta^3}\ .\end{aligned} \tag{56}$$

It might be more useful to rewrite this expression in terms of the mean number density per unit redshift and per unit solid angle $dN(z)/dz$, which is defined by $dN(z) = \tilde{n}^{\rm S}(s)s^2 ds = \tilde{n}^{\rm R}(r)r^2 dr$,

$$P_{\rm S}^{\rm LC}(k) \simeq \frac{\displaystyle\int dz \left(\frac{dz}{ds}\right) \frac{1}{s^2}\left(\frac{dN}{dz}\right)^2 D_1[z]^2 \int_0^1 d\mu P\Big(\frac{k}{\Theta}\Big) \frac{b\Big[k/\Theta; z\Big]^2}{\Theta^3}}{\displaystyle\int dz \left(\frac{dz}{ds}\right) \frac{1}{s^2}\left(\frac{dN}{dz}\right)^2}\ , \tag{57}$$

where s is regarded as a function of z specified by the relation $\bar{a}(\bar{\eta}_0 - s) = 1/(1+z)$.

4.3. Validity of approximation and implications

We show how the cosmological redshift-space distortion distorts the power spectrum on a light cone. In this section we adopt the same galaxy and quasar samples as in subsection 3.4. We take $\Omega_0 = 0.3$ as the density parameter of the real space (the 'correct' universe). And we adopt $\bar{\Omega}_0 = 1.0$ as that of the redshift space. In this section, we assume that $h = \bar{h} = 0.7$ for the real and the redshift spaces for simplicity. [3]

The exact power spectrum which takes the cosmological redshift-space distortion into account is computed from equation (12) by integrating the exact two-point correlation function (50). The approximate formula is given by equation (56) or (57). Figure 5 plots the galaxy power spectra. Figure 6 shows the case of the quasars. The solid and the dotted lines represent the exact and the approximate power spectra, respectively. It is apparent from the figures that the approximate formula shows the good correspondence with the exact formula for $k \gtrsim 0.01h\mathrm{Mpc}^{-1}$. The exact power spectrum approaches a constant value at the large scale, and the deviation of the exact formula from the approximate formula becomes large for $k \lesssim 0.01\ h\mathrm{Mpc}^{-1}$. This is caused by the finite size effect of the survey volume, as mentioned in subsection 3.5.

In Figures 5 and 6, the short dashed line shows the power spectrum defined on the constant-time hypersurface at present $P(k)b_0^2$. In lower panels, the power spectrum, divided by the power spectrum at present, $P_{\mathrm{S}}^{\mathrm{LC}}(k)/P(k)b_0^2$, is plotted. Although we here adopted the scale-independent bias model, the distortion of the power spectrum depends on the scale k. The location of the peak of the power spectrum is moved, due to the redshift-space distortion. Thus the cosmological redshift-space distortion distorts the power spectrum by shifting the wavenumber k, which is expected from the expression (56) or (57). This feature is in marked contrast to the case of the linear redshift-space distortion (see equation [36] and Figure 3).

The long dashed line plots the case $\Omega_0 = \bar{\Omega}_0 = 0.3$, which is labeled by $P_{\mathrm{R}}^{\mathrm{LC}}(k)$. That is, the long dashed line shows the case when the cosmological redshift-space distortion is not effective, and it merely shows a contribution from the light-cone effect. Comparing the solid line and the long dashed line in the lower panels, we conclude that the cosmological redshift-space distortion is an important effect not only for the quasar sample but also for the galaxy sample in estimating the power spectrum. The cosmological redshift-space distortion affects the power spectrum at the 10 percent level for the galaxy sample. For the quasar samples, the effect becomes more significant. Moreover we should note that the behavior significantly depends on the time-evolution of the bias model.

---

[3]The difference of the Hubble parameter can cause an additional difference in the power spectra which is not essential to the cosmological redshift-space distortion. Therefore we here choose $h = \bar{h}$ for definiteness.

5. CONCLUSIONS

In the present paper, we investigated the power spectrum of cosmological objects on a light cone focusing on the redshift-space distortions in linear theory of density perturbations. We developed theoretical formulations to compute the power spectrum which properly takes into account the light-cone effect and the redshift-space distortion effects. The linear and the cosmological redshift-space distortions were considered in section 3 and 4, respectively. The formulae for the power spectra were derived in the rigorous manner starting from the first principle corresponding to the Fourier analysis. Using the distant observer approximation, we derived the approximate formulae (eqs.[36] and [56]), and examined the validity and the limitations. It was shown that the approximate expressions are useful to describe the effects properly.

Applying our formulae to galaxy and quasar samples which roughly match the SDSS survey, we showed that the effects considered in the present paper become important for on-going wide and deep surveys like the SDSS and 2dF surveys. Let us summarize the results and the implications obtained in this paper. For the galaxy samples, the light-cone effect decreases the amplitude of the power spectrum several percentage points; the cosmological redshift-space distortion can distort the power spectrum by order of ten percent; and the linear redshift-space distortion increases the amplitude by order of several $\times 10$ percent, depending on the cosmological parameters. The power spectrum is rather insensitive to the time-evolution of the bias model for the shallow galaxy samples (Paper Ⅲ). For the quasar samples, the linear redshift-space distortion can be a minor effect, and the light-cone effect and the cosmological redshift-space distortion are the influential effects. Of course the power spectrum significantly depends on the cosmological model and the bias model.

In the present paper we have shown the validity of using the approximate formulas at the small scales. Our numerical calcuations have shown that the approximate formulas become invalid at the large scales for $k \lesssim 0.01h\mathrm{Mpc}^{-1}$. Let us briefly discuss the physical meaning of the discrepancy between the exact formula and the approximate formula. The terminology, exact, means that the formulas are derived from the definitions of the statistical estimator for the two-point correlation function and the power spectrum, which corresponds to a conventional data processing. Then the exact formulas indicate how the finite size effect of the survey volume affects the two-point correlation function and the power spectrum. For the two-point correlation function the finite size effect decreases the amplitude of the correlation function at the large scales. For example the amplitude becomes zero for $R \geq 2r_{\mathrm{max}}$, where $2r_{\mathrm{max}}$ is the diameter of the survey volume (see Figure 1). For the large separation (for large R), the sign of the two-point correlation function is negative, which implies the anti-correlation at the large scales. Thus the finite size effect decreases the anti-correlation at the large scales. We suppose that this causes the large amplification of the power spectra at the large scales (at small k) relative to its counterpart in linear theory.

Because we worked in linear theory in the present paper, the behaviors on small scales (at

large k) are not correctly described, where the nonlinear effect causes an additional distortion of the power spectrum. The distortion of the power spectrum was discussed by extending the formula to incorporate the nonlinear effect in Paper Ⅲ, though the exact derivation was invalidated by the inclusion of the nonlinear effect in a strict sense. According to the result, the nonlinear effect causes the additional distortion of the power spectrum by order of several $\times 10$ percent at $0.1h\mathrm{Mpc}^{-1} \lesssim k \lesssim 1h\mathrm{Mpc}^{-1}$, depending on the cosmological model. In the present paper, the linear redshift-space distortion and the cosmological redshift-space distortion are discussed separately, however, investigations combining these effects are needed to present realistic theoretical predictions. (Suto, Magira, & Yamamoto 1999). Moreover we note that the bias model is the crucial problem to present precise theoretical predictions for the power spectrum (Moscardini, et al. 1998; Dekel & Lahav 1999; Taruya, Koyama, & Soda 1999; Tegmark & Peebles 1998), though we here adopted a simple model.

ACKNOWLEDGMENTS

We are grateful to Yasufumi Kojima for useful discussions and comments. We thank Yasushi Suto for his useful discussions, instructions, and for providing numerical routines to compute quasar selection functions. We also thank Silvio Perez for carefully reading the manuscript. Numerical computations were carried out in part on INSAM of Hiroshima University. This research was supported by the Inamori Foundation and in part by the Grants-in-Aid program (11640280) by the Ministry of Education, Science, Sports and Culture of Japan.

APPENDIX

A. Brief summary of the calculation $\xi_{\rm S}^{\rm LC}(R)$

We here briefly outline the calculation of equation (29). We use the almost same mathematical notations as those in Paper II, in which similar calculations have been given. The calcuations in Paper II will supplement arguments in this Appendix. We work within a framework of linear theory of density perturbations based on the CDM cosmological model. We expand the CDM density contrast δ_c and the velocity field v_c^i in terms of the scalar harmonics as follows (e.g., Kodama & Sasaki 1984)

$$\delta_c(\eta,\chi,\boldsymbol{\gamma}) = \int_0^\infty dk \sum_{l,m} \delta_{klm}^{(\rm c)}(\eta)\mathcal{Y}_{klm}(\chi,\boldsymbol{\gamma}), \tag{A1}$$

$$v_c^i(\eta,\chi,\boldsymbol{\gamma}) = \int_0^\infty dk \sum_{l,m} \frac{\dot{\delta}_{klm}^{(\rm c)}(\eta)}{k^2}\mathcal{Y}_{klm}(\chi,\boldsymbol{\gamma})^{|i}, \tag{A2}$$

where $\mathcal{Y}_{klm}(\chi,\boldsymbol{\gamma})$ is the normalized scalar harmonics

$$\mathcal{Y}_{klm}(\chi,\boldsymbol{\gamma}) = X_k^l(\chi)Y_{lm}(\Omega\boldsymbol{\gamma}), \tag{A3}$$

with

$$X_k^l(\chi) = \sqrt{\frac{2}{\pi}}kj_l(k\chi), \tag{A4}$$

and $Y_{lm}(\Omega\boldsymbol{\gamma})$ and $j_l(x)$ are the spherical harmonics and the spherical Bessel function, respectively, and $\mathcal{Y}_{klm}(\chi,\boldsymbol{\gamma})^{|i}$ denotes the covariant derivative of $\mathcal{Y}_{klm}(\chi,\boldsymbol{\gamma})$ on the three-dimensional space. The Fourier coefficient $\delta_{klm}^{(\rm c)}(\eta)$ satisfies

$$\ddot{\delta}_{klm}^{(\rm c)} + \frac{\dot{a}}{a}\dot{\delta}_{klm}^{(\rm c)} - \frac{3}{2}\frac{\Omega_0 H_0^2}{a}\delta_{klm}^{(\rm c)} = 0. \tag{A5}$$

In the Friedmann-Lemaitre universe, the growing mode solution is well known:

$$\delta_{klm}^{(\rm c)}(\eta) = \delta_{klm}^{(\rm c)}(\eta_0)D_1(a), \tag{A6}$$

with

$$D_1(a) = A\sqrt{\frac{\Omega_0}{a^3}+1-\Omega_0}\int_0^a da'\Big(\frac{a'}{\Omega_0+a'^3(1-\Omega_0)}\Big)^{3/2}. \tag{A7}$$

Here A is a constant to be determined so that D_1 is unity at present.

We assume that the number density contrast of objects connects with the CDM density contrast by the scale-dependent bias factor $b(k;\eta)$ as,

$$\Delta_{klm}(\eta) = b(k;\eta)\delta_{klm}^{(c)}(\eta). \tag{A8}$$

Furthermore we assume that the velocity field of the objects, $\boldsymbol{v}(\eta,\chi,\boldsymbol{\gamma})$, is the same as that of CDM $\boldsymbol{v}_c(\eta,\chi,\boldsymbol{\gamma})$. In this case the apparent shift of comoving distance of an object, $\delta r(r,\boldsymbol{\gamma})$, is related to the velocity as

$$\delta r(r,\boldsymbol{\gamma}) = \frac{a(\eta)^{\frac{1}{2}}}{H_0\sqrt{\Omega_0+\Omega_\lambda a(\eta)^3}}\boldsymbol{\gamma}\cdot\boldsymbol{v}_c(\eta,\chi,\boldsymbol{\gamma})\Big|_{\eta\to\eta_0-r,\chi\to r}\ . \tag{A9}$$

With these assumptions we write

$$\Delta^{\rm R}(r,\boldsymbol{\gamma}) = \int_0^\infty dk\sum_{lm}\delta^{(\rm c)}_{klm}(\eta_0)b(k;\eta_0-r)D_1(\eta_0-r)\mathcal{Y}_{klm}(r,\boldsymbol{\gamma}), \tag{A10}$$

$$\delta r(r,\boldsymbol{\gamma}) = \int_0^\infty dk\sum_{lm}\delta^{(\rm c)}_{klm}(\eta_0)f(\eta_0-r)D_1(\eta_0-r)k^{-2}\mathcal{Y}_{klm}(r,\boldsymbol{\gamma})^{|r}, \tag{A11}$$

where

$$f(\eta) = \frac{d\ln D_1(\eta)}{d\ln a(\eta)}\ . \tag{A12}$$

Substituting equations (A10) and (A11) into (28), we obtain

$$\begin{aligned}\xi^{\rm LC}_{\rm S}(R) &= \left[\int d^3\boldsymbol{r}\tilde{n}^{\rm R}(r)^2\right]^{-1}\int\frac{d\Omega_{\hat{\boldsymbol{R}}}}{4\pi}\int dr_1r_1^2d\Omega_{\boldsymbol{\gamma}_1}\int dr_2r_2^2d\Omega_{\boldsymbol{\gamma}_2}\\
&\times\tilde{n}^{\rm R}(r_1)\tilde{n}^{\rm R}(r_2)D_1(\eta_0-r_1)D_1(\eta_0-r_2)\\
&\times\int_0^\infty dk_1\sum_{l_1m_1}\int_0^\infty dk_2\sum_{l_2m_2}\left\langle\delta^{(\rm c)}_{k_1l_1m_1}(\eta_0)\delta^{(\rm c)*}_{k_2l_2m_2}(\eta_0)\right\rangle Y_{l_1m_1}(\Omega_{\boldsymbol{\gamma}_1})Y^*_{l_2m_2}(\Omega_{\boldsymbol{\gamma}_2})\\
&\times\prod_{i=1}^2\left\{\left[b(k_i;\eta_0-r_i)-k_i^{-2}\mathcal{D}_{r_i}\right]X^{l_i}_{k_i}(r_i)\right\}\delta^{(3)}(\boldsymbol{r}_1-\boldsymbol{r}_2-\boldsymbol{R}),\end{aligned} \tag{A13}$$

where

$$\mathcal{D}_r = f(\eta_0-r)\frac{d}{dr}\ln\left[r^2\tilde{n}^{\rm R}(r)f(\eta_0-r)D_1(\eta_0-r)\right]\frac{\partial}{\partial r}+f(\eta_0-r)\frac{\partial^2}{\partial r^2}. \tag{A14}$$

Using the relation

$$e^{i\boldsymbol{k}\cdot\boldsymbol{r}} = 4\pi\sum_l\sum_{m=-l}^{l}(-i)^ij_l(k|\boldsymbol{r}|)Y_{lm}(\Omega_{\hat{\boldsymbol{k}}})Y^*_{lm}(\Omega_{\hat{\boldsymbol{r}}}), \tag{A15}$$

equation (A13) is written as

$$\begin{aligned}\xi^{\rm LC}_{\rm S}(R) &= \left[\int d^3\boldsymbol{r}\tilde{n}^{\rm R}(r)^2\right]^{-1}\int\frac{d\Omega_{\hat{\boldsymbol{R}}}}{4\pi}\int dr_1r_1^2d\Omega_{\boldsymbol{\gamma}_1}\int dr_2r_2^2d\Omega_{\boldsymbol{\gamma}_2}\\
&\times\tilde{n}^{\rm R}(r_1)\tilde{n}^{\rm R}(r_2)D_1(\eta_0-r_1)D_1(\eta_0-r_2)\\
&\times\int_0^\infty dk_1\sum_{l_1m_1}\int_0^\infty dk_2\sum_{l_2m_2}\left\langle\delta^{(\rm c)}_{k_1l_1m_1}(\eta_0)\delta^{(\rm c)*}_{k_2l_2m_2}(\eta_0)\right\rangle Y_{l_1m_1}(\Omega_{\boldsymbol{\gamma}_1})Y^*_{l_2m_2}(\Omega_{\boldsymbol{\gamma}_2})\\
&\times\frac{2}{\pi}\prod_{i=1}^2\left\{\left[b(k_i;\eta_0-r_i)-k_i^2\mathcal{D}_{r_i}\right]k_ij_{l_i}\right\}\end{aligned}$$

$$\times\frac{1}{(2\pi)^3}\int d^3\boldsymbol{k}4\pi\sum_{L_1M_1}(-i)^{L_1}j_{L_1}(kr_1)Y_{L_1M_1}(\Omega_{\hat{\boldsymbol{k}}})Y^*_{L_1M_1}(\Omega_{\boldsymbol{\gamma}_1})$$
$$\times4\pi\sum_{L_2M_2}(i)^{L_2}j_{L_2}(kr_2)Y^*_{L_2M_2}(\Omega_{\hat{\boldsymbol{k}}})Y_{L_2M_2}(\Omega_{\boldsymbol{\gamma}_2})$$
$$\times4\pi\sum_{L_3M_3}(i)^{L_3}j_{L_3}(kR)Y^*_{L_3M_3}(\Omega_{\hat{\boldsymbol{k}}})Y_{L_3M_3}(\Omega_{\hat{\boldsymbol{R}}})\ , \tag{A16}$$

where $k=|\boldsymbol{k}|$ and $\hat{\boldsymbol{k}}=\boldsymbol{k}/k$. Integration over $\Omega_{\boldsymbol{\gamma}_1}$, $\Omega_{\boldsymbol{\gamma}_2}$, $\Omega_{\hat{\boldsymbol{R}}}$, and $\Omega_{\hat{\boldsymbol{k}}}$ yields

$$\begin{aligned}\xi^{\rm LC}_{\rm S}(R) &= \left[\int d^3\mathbf{r}\tilde{n}^{\rm R}(r)^2\right]^{-1}\int dr_1r_1^2\int dr_2r_2^2\tilde{n}^{\rm R}(r_1)\tilde{n}^{\rm R}(r_2)D_1(\eta_0-r_1)D_1(\eta_0-r_2)\\
&\times\int_0^\infty dk_1\sum_{l_1m_1}\int_0^\infty dk_2\sum_{l_2m_2}\left\langle\delta^{\rm (c)}_{k_1l_1m_1}(\eta_0)\delta^{\rm (c)*}_{k_2l_2m_2}(\eta_0)\right\rangle\\
&\times\frac{2}{\pi}\prod_{i=1}^2\left\{\left[b(k_i;\eta_0-r_i)-k_i^{-2}\mathcal{D}_{r_i}\right]k_ij_{l_i}(k_ir_i)\right\}\\
&\times\frac{(4\pi)^2}{(2\pi)^3}\int dkk^2j_{l_1}(kr_1)j_{l_2}(kr_2)j_0(kR)\delta_{l_1,l_2}\delta_{m_1,m_2}\ .\end{aligned}\tag{A17}$$

Because the Gaussian random fluctuations satisfy

$$\left\langle\delta^{\rm (c)}_{k_1l_1m_1}(\eta_0)\delta^{\rm (c)*}_{k_2l_2m_2}(\eta_0)\right\rangle=\delta(k_1-k_2)\delta_{l_1l_2}\delta_{m_1m_2}P(k_1),\tag{A18}$$

where $P(k)$ is the CDM power spectrum at present, we obtain

$$\begin{aligned}\xi^{\rm LC}_{\rm S}(R) &= \left[\int d^3\boldsymbol{r}\tilde{n}^{\rm R}(r)^2\right]^{-1}\int dr_1r_1^2\int dr_2r_2^2\tilde{n}^{\rm R}(r_1)\tilde{n}^{\rm R}(r_2)D_1(\eta_0-r_1)D_1(\eta_0-r_2)\\
&\times\frac{4}{\pi^2}\int_0^\infty dk_1k_1^2P(k_1)\sum_l(2l+1)\prod_{i=1}^2\left\{\left[b(k_1;\eta_0-r_i)-k_1^{-2}\mathcal{D}_{r_i}\right]j_l(k_1r_i)\right\}\\
&\times\int dkk^2j_l(kr_1)j_l(kr_2)j_0(kR)\ .\end{aligned}\tag{A19}$$

By using the mathematical formulae, (Magnus et al. 1966)

$$\int dkk^2j_l(kr_1)j_l(kr_2)j_0(kR)=\begin{cases}\frac{\pi}{4r_1r_2R}P_l\left(\frac{r_1^2+r_2^2-R^2}{2r_1r_2}\right) & (|r_1-r_2|<R<r_1+r_2),\\ 0 & (R<|r_1-r_2|,R>r_1+r_2),\end{cases}\tag{A20}$$

and

$$\sum_l(2l+1)P_l(\cos\theta)j_l(kr_1)j_l(kr_2)=j_0\left(k\sqrt{r_1^2+r_2^2-2r_1r_2\cos\theta}\right),\tag{A21}$$

we find

$$\begin{aligned}\xi^{\rm LC}_{\rm S}(R) &= \left[\int d^3\boldsymbol{r}\tilde{n}^{\rm R}(r)^2\right]^{-1}\frac{1}{\pi R}\iint_{\mathcal{S}}dr_1dr_2r_1r_2\tilde{n}^{\rm R}(r_1)\tilde{n}^{\rm R}(r_2)D_1(\eta_0-r_1)D_1(\eta_0-r_2)\\
&\times\int_0^\infty dkk^2P(k)\prod_{i=1}^2\left[b(k;\eta_0-r_i)-k^{-2}\mathcal{D}_{r_i}\right]j_0\left(k\sqrt{r_1^2+r_2^2-2r_1r_2\cos\theta}\right)\ ,\end{aligned}\tag{A22}$$

where $\mathcal{S}$ denotes the region $|r_1-r_2| \le R \le r_1+r_2$, and $\cos\theta$ is replaced by $\cos\theta = (r_1^2+r_2^2-R^2)/2r_1r_2$ after operating the differentiations with respect to r_1 and r_2.

Using the formulae, (B17)-(B19) in Paper II, and omitting the second term in the derivative, i.e., approximating as $\mathcal{D}_r \simeq f(\eta_0 - r)\partial^2/\partial r^2$, we finally have

$$\begin{aligned}
\xi_{\rm S}^{\rm LC}(R) &= \left[\int dr r^2 \tilde{n}^{\rm R}(r)^2\right]^{-1} \frac{1}{2R} \iint_{\mathcal{S}} dr_1 dr_2 r_1 r_2 \tilde{n}^{\rm R}(r_1)\tilde{n}^{\rm R}(r_2) \\
&\quad \times \frac{1}{2\pi^2}\int dk k^2 P(k) \prod_{i=1}^{2}\Big[b(k;\eta_0-r_i)D_1(\eta_0-r_i)\Big] \\
&\quad \times \Big[j_0(kR) + \beta(k;\eta_0-r_2)I(k;R;r_1,r_2) + \beta(k;\eta_0-r_1)I(k;R;r_2,r_1) \\
&\quad + \beta(k;\eta_0-r_1)\beta(k;\eta_0-r_2)J(k;R;r_1,r_2)\Big], \qquad \text{(A23)}
\end{aligned}$$

where

$$I(k;R;r_1,r_2) = \frac{j_1(kR)}{kR} - \frac{j_2(kR)}{R^2}\left\{\frac{R^2+r_2^2-r_1^2}{2r_2}\right\}^2 \qquad \text{(A24)}$$

$$\begin{aligned}
J(k;R;r_1,r_2) &= \frac{j_2(kR)}{(kR)^2}\left[2\left\{\frac{r_1^2+r_2^2-R^2}{2r_1r_2}\right\}^2 + 1\right] \\
&\quad + \frac{j_4(kR)}{R^4}\left\{\frac{R^2+r_1^2-r_2^2}{2r_1}\right\}^2\left\{\frac{R^2+r_2^2-r_1^2}{2r_2}\right\}^2 \\
&\quad - \frac{j_3(kR)}{kR^3}\left[\left\{\frac{R^2+r_1^2-r_2^2}{2r_1}\right\}^2 + \left\{\frac{R^2+r_2^2-r_1^2}{2r_2}\right\}^2\right. \\
&\quad \left. - \frac{R^2+r_1^2-r_2^2}{r_1}\frac{R^2+r_2^2-r_1^2}{r_2}\frac{r_1^2+r_2^2-R^2}{2r_1r_2}\right], \qquad \text{(A25)}
\end{aligned}$$

and $\beta(k;\eta_0-r)$ is defined by equation (30). Equation (A23) is identical to equation (29).

REFERENCES

Alcock, C., & Paczynski, B. 1979, Nature, 281, 358

Ballinger, W. E., Peacock, J. A., & Heavens, A. F. 1996, MNRAS, 282, 877

Bardeen, J. M., Bond, J. R., Kaiser, N., & Szalay, A. S. 1986, ApJ, 304, 15

Cole, S., Fisher, K. B., & Weinberg, D. H. 1995, MNRAS, 275, 515

Davis, M., & Peebles, P. J. E. 1983, ApJ, 267, 465

Dekel, A., & Lahav, O. 1999, ApJ, 520, 24

de Laix ,A. A., & Starkman, G. D. 1998, MNRAS, 299, 977

Feldman, H. A., Kaiser, N., & Peacock, A. A. 1994, ApJ, 426, 23

Fry, J. N. 1996, ApJ, 461, L65

Hamilton, A. J. S. 1998, in " The Evolving Universe. Selected Topics on Large-Scale Structure and on the Properties of Galaxies", (Kluwer: Dordrecht), p.185.

Kaiser, N. 1987, MNRAS, 277, 1

Kitayama, J., & Suto, Y. 1997, ApJ, 490, 557

Kodama, H., & Sasaki, M. 1984, Prog. Theor. Phys. Supp., 78, 1

Loveday, J., Peterson, B. A., Efsathiou, G., & Maddox, S.J. 1992, ApJ, 390, 338

Magira, H., Jing, Y. P., & Suto, Y. 1999, ApJ, in press.

Magnus, W., Oberhettinger, F., & Soni, R. P. , Formulae and Theorems for the Special Functions of Mathematical Physics, P.426 (Springer-Verlag, Belrin: 1966)

Matarrese, S., Coles, P., Lucchin, F., & Moscardini, L 1997, MNRAS, 286, 115

Matsubara, T. 1999, astro-ph/9908056.

Matsubara, T., Suto, Y., & Szapdi, I. 1997, ApJ, 491, L1

Matsubara, T., & Suto, Y. 1996, ApJ, 470, L1

Moscardini, L., Coles, P., Lucchin, F., & Matarrese, S. 1998, MNRAS, 299, 95

Nakamura, T. T., Matsubara, T., & Suto, Y. 1998, ApJ, 494, 13

Nakamura, T. T., & Suto, Y. 1997, Prog. Theor. Phys., 97, 49

Nishioka, H., & Yamamoto, K. 1999, ApJ, 520, 426 (Paper II)

Ryden, B. S. 1995, ApJ, 452, 25

Sugiyama, N. 1995, ApJS, 100, 281

Suto, Y., Magira, H., Jing, Y. P., Matsubara, T., & Yamamoto, K. 1999, Prog. Theor. Phys. Supp., 133, 183

Suto, Y., Magira, H., & Yamamoto, K. 1999, submitted to PASJ.

Szalay, A.S., Matsubara, T., & Landy, S.D. 1998, ApJ, 498, L1

Taruya, A., Koyama, K., & Soda, J. 1999, ApJ, 510, 541

Wallington, S., & Narayan, R. 1993, ApJ, 403, 517

Yamamoto, K., & Suto, Y. 1999, ApJ, 517, 1 (Paper I)

Yamamoto, K., Nishioka, H., & Suto, Y. 1999, ApJ in press (Paper III).

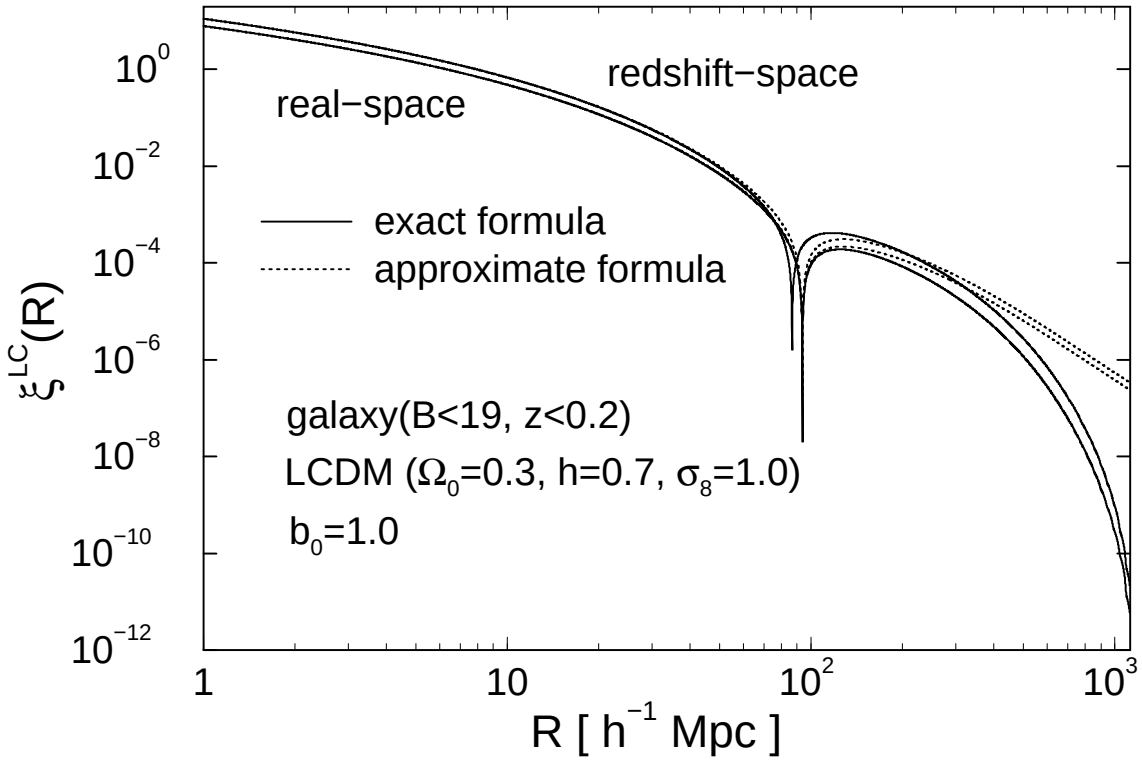

Fig. 1.— The two-point correlation functions on a light cone for galaxy sample in real and redshift spaces. The solid line represents the exact formula (29) and the dotted line represents the approximate formula (34). Upper pair curves correspond to the case that the linear redshift-space distortion is taken into account by using formulae (29) and (34). Lower pair curves correspond to the case of the real space by setting $\beta = 0$ in (29) and (34).

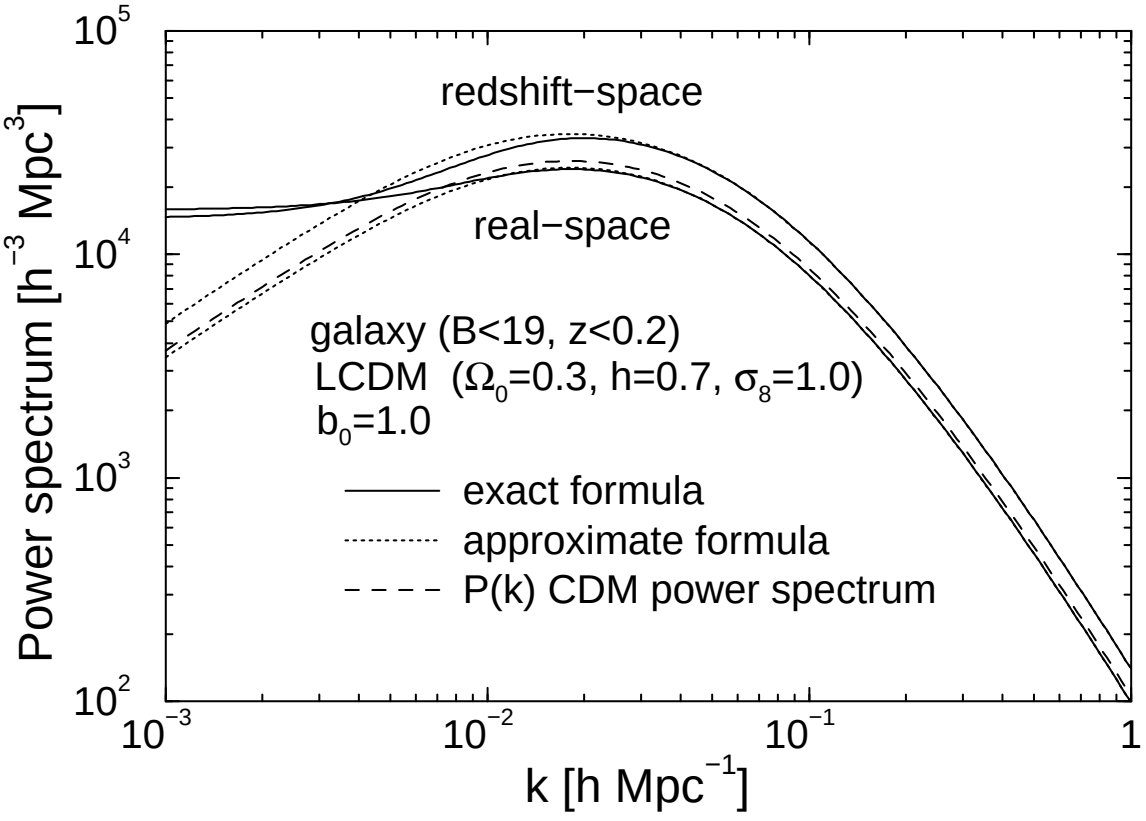

Fig. 2.— The power spectra on a light cone for galaxy sample in real and redshift spaces. The solid line represents the exact power spectrum and the dotted line represents the approximate formula (36). Upper pair curves correspond to the case that the linear redshift-space distortion is taken into account, $P_{\rm S}^{\rm LC}(k)$. Lower pair curves correspond to the case in real space, $P_{\rm R}^{\rm LC}(k)$. (Here we refer the 'real space' to the case $\beta(k;\eta) = 0.$ in the formulae.) The dashed line corresponds to the CDM power spectrum defined on a constant-time hypersurface at present $P(k)$.

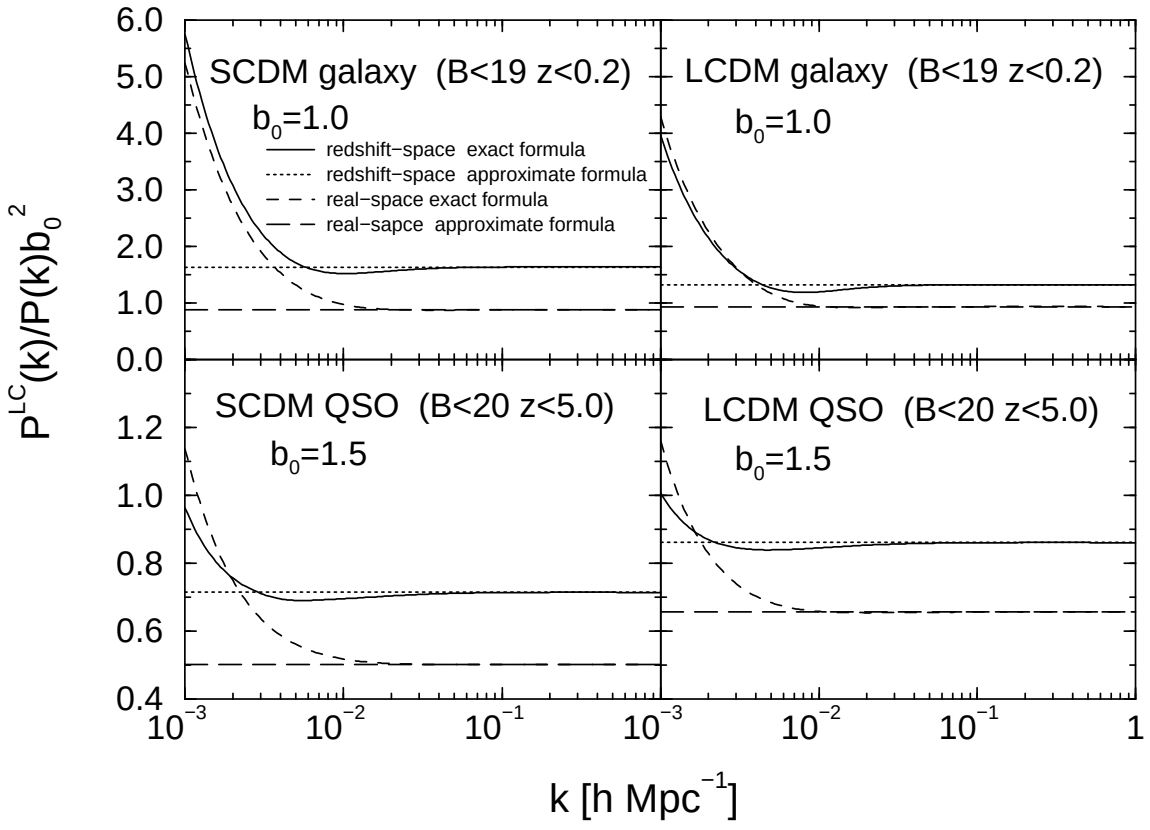

Fig. 3.— Real and redshift space power spectra for galaxy and quasar samples, divided by power spectra of galaxy and quasar on a constant-time hypersurface at present, for SCDM and LCDM models. The solid line and dotted line represent the exact and approximate power spectra in redshift space, respectively. The short and long dashed lines express the exact and the approximate power spectra in real space, respectively. We adopted the bias model with $b_0 = 1$ for galaxies, and $b_0 = 1.5,\ p = 1$ for quasars.

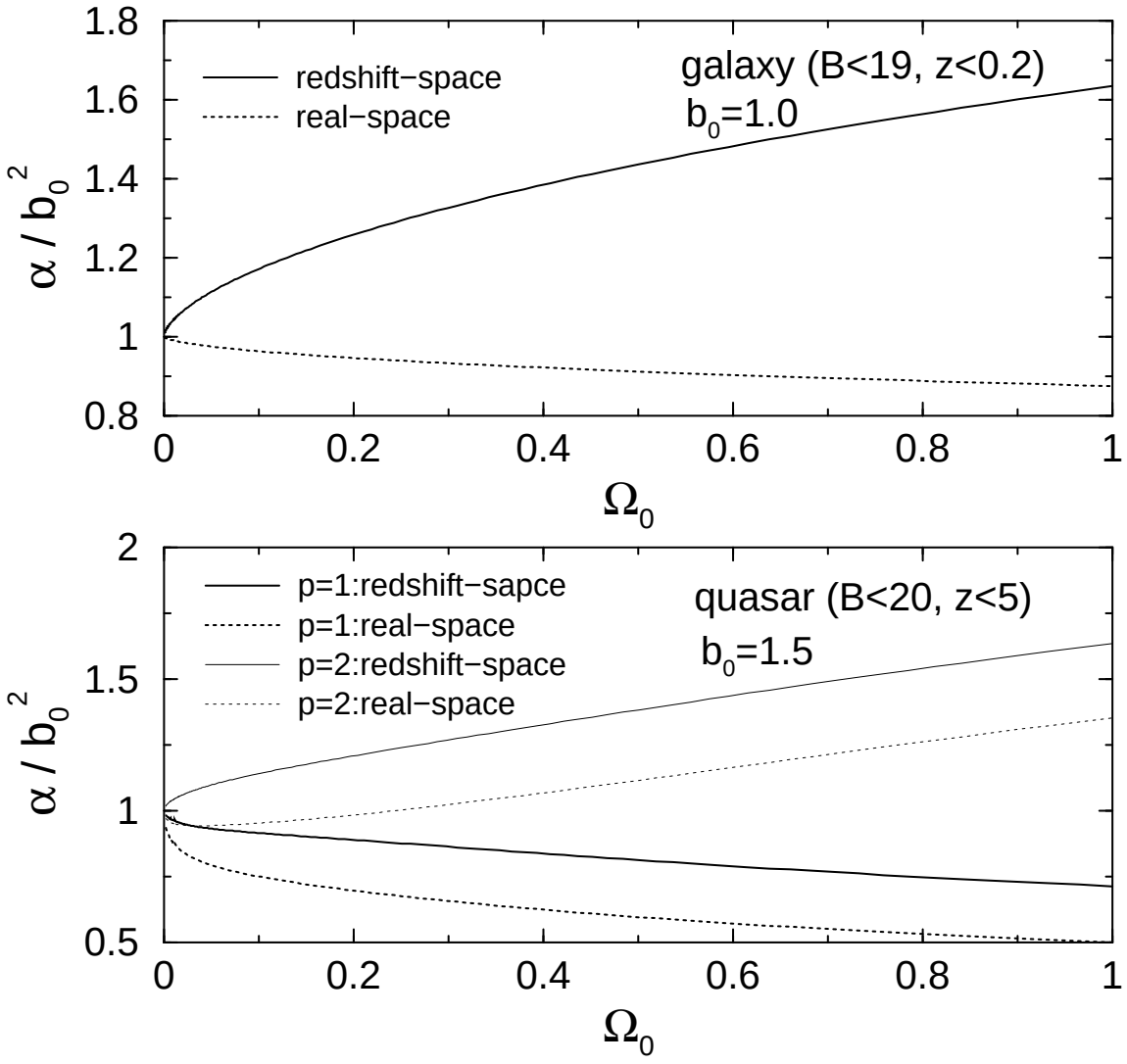

Fig. 4.— The factor α/b_0^2 for galaxy and quasar as a function of Ω_0. The solid and the dotted lines represent the factor in redshift and real spaces, respectively. The case of real space is defined by the case $\beta = 0$ in the formulae. As for the bias, we adopt the model with $b_0 = 1$ for galaxy, and $b_0 = 1.5,$ and $p = 1,\ 2$ for quasar.

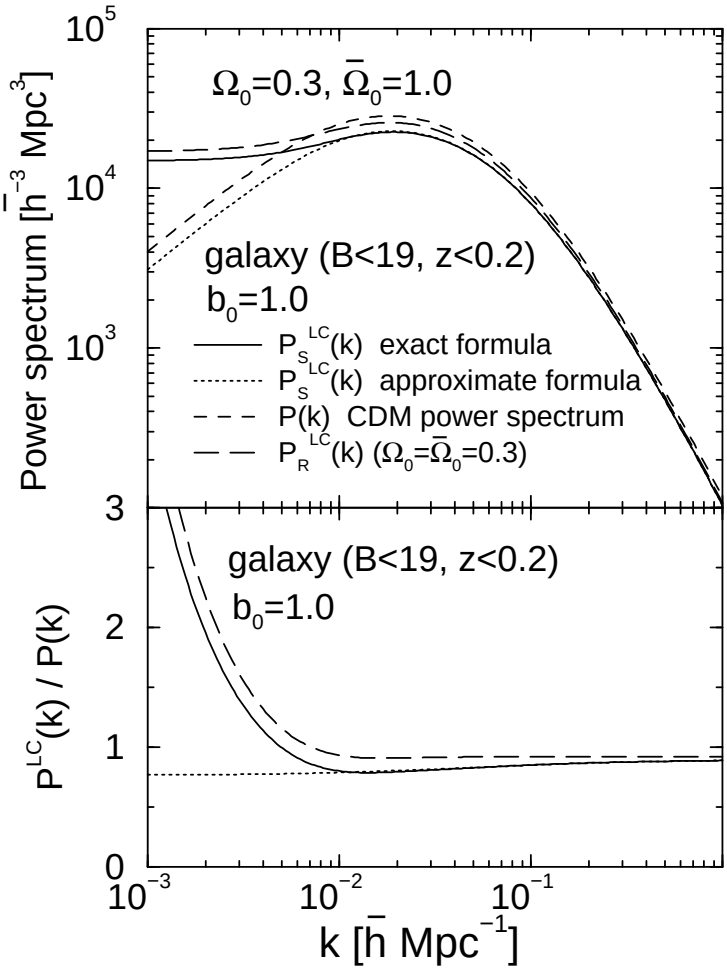

Fig. 5.— Galaxy power spectrum on a light cone which incorporates the cosmological redshift-space distortion. Here we adopted the galaxy sample in subsection 3.4, and $(\Omega_0 = 0.3, h = 0.7)$, and $(\bar{\Omega}_0 = 1.0,\ \bar{h} = 0.7)$. The case of no bias is considered. The solid and dotted line represent the exact and the approximate power spectra, respectively. The short dashed line plots the power spectrum on a constant-time hypersurface and the long dashed line labeled by $P_{\rm R}^{\rm LC}(k)$ does the power spectrum assuming the correct cosmological model in redshift space, i.e., $(\Omega_0 = \bar{\Omega}_0 = 0.3)$. Thus the long dashed line merely expresses the decrease of the power spectrum due to light-cone effect. The upper panel shows the power spectra, and the lower panel shows the power spectra divided by the power spectrum on the constant-time hypersurface at present, $P(k)$.

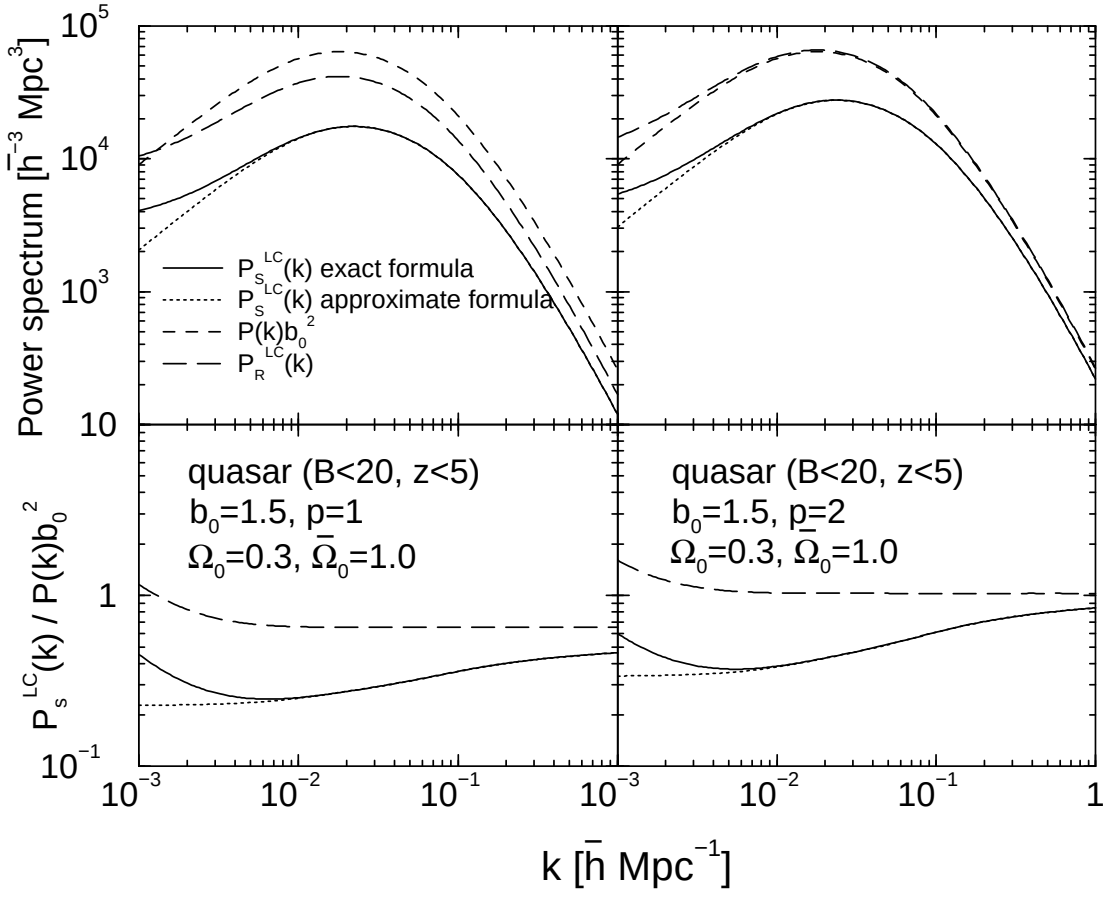

Fig. 6.— Quasar power spectra on a light cone which take the cosmological redshift-space distortion into account. We adopted the quasar sample in subsection 3.4, and $\Omega_0 = 0.3$, $h = 0.7$, and $\bar{\Omega}_0 = 1.0$, $\bar{h} = 0.7$. Here the bias model with $b_0 = 1.5$, and $p = 1,\ 2$ is considered. The meanings of the lines are the same as Figure 5.